A&A, 709, A44 (2026)
https://doi.org/10.1051/0004-6361/202658849

Astronomy & Astrophysics

High-contrast imaging of Galactic Cepheids with VLT/SPHERE

A. Gallenne[1,⋆], P. Kervella[2,3], N. R. Evans[4], J. Milli[5], E. Sivkova[2,3], W. Gieren[6], G. Pietrzyński[7], G. Bras[2], V. Hocdé[8], W. Kiviaho[2,3], N. Nardetto[8], B. Pilecki[7], and B. Zgirski[6]

[1] Instituto de Alta Investigación, Universidad de Tarapacá, Casilla 7D, Arica, Chile
[2] LIRA, Observatoire de Paris, Université PSL, Sorbonne Université, Université Paris Cité, CY Cergy Paris Université, CNRS, 5 Place Jules Janssen, 92195 Meudon, France
[3] French-Chilean Laboratory for Astronomy, IRL 3386, CNRS and U. de Chile, Casilla 36-D, Santiago, Chile
[4] Smithsonian Astrophysical Observatory, MS 4, 60 Garden Street, Cambridge, MA 02138, USA
[5] Univ. Grenoble Alpes, CNRS, IPAG, 38000 Grenoble, France
[6] Universidad de Concepción, Departamento de Astronomía, Casilla 160-C, Concepción, Chile
[7] Centrum Astronomiczne im. Mikołaja Kopernika, PAN, Bartycka 18, 00-716 Warsaw, Poland
[8] Université Côte d'Azur, Observatoire de la Côte d'Azur, CNRS, Laboratoire Lagrange, Nice, France

Received 2 January 2026 / Accepted 12 March 2026

ABSTRACT

Context. Classical Cepheids are key distance indicators and benchmarks for stellar evolution, yet most of them are members of binary or multiple systems. While spectroscopic surveys and *Gaia* proper-motion anomalies reveal a high binary fraction, the population of resolved companions remains poorly characterised.
Aims. We aim to search for and characterise visual companions to bright Galactic Cepheids using high-contrast imaging and to derive quantitative limits on undetected companions to constrain the architecture of Cepheid multiple systems.
Methods. We observed 47 Galactic Cepheids with VLT/SPHERE using the ZIMPOL instrument in classical imaging mode and the V, R', and I' filters. The data were obtained in pupil-stabilised mode and analysed using PCA-based imaging technique. For detected companions, we injected negative fake companions in a Monte Carlo approach to measure the relative astrometry. For non-detections, synthetic companions were injected to compute 5σ contrast curves as a function of separation.
Results. We detected companions with a signal-to-noise ratio of S/N > 5 for eight Cepheids (η Aql, AX Cir, S Nor, AP Pup, W Sgr, T Vel, TX Del, and V659 Cen), corresponding to about 17% of the sample. Our SPHERE imaging confirms previously known visual companions with improved astrometry and reveals new wide components for AP Pup, T Vel, and TX Del) at projected separations of ∼0.16–0.9″. For the remaining Cepheids, we derived typical maximum contrasts of ∼10, 11, and 12 mag at 0.25″, 0.5″, and >1″, respectively. For a sub-set of targets, these limits ruled out main sequence companions more massive than late-K dwarfs beyond 0.5″.
Conclusions. Our SPHERE survey provides the first homogeneous set of high-contrast optical constraints on wide companions of Galactic Cepheids. The low detection rate of visual companions compared to the high overall binary fraction implies that most companions inferred from radial velocities and *Gaia* astrometry are either closer than ∼20 mas or significantly fainter than the limits reached here.

Key words. instrumentation: high angular resolution – binaries: visual – stars: variables: Cepheids

1. Introduction

Classical Cepheids are pulsating evolved stars that are widely used as standard candles to estimate distances in nearby galaxies. Beyond their utility in terms of the cosmic distance scale with the period-luminosity relation (PLR), they are also powerful astrophysical laboratories, providing fundamental clues for studying the pulsation and evolution of intermediate-mass stars. The physics of classical Cepheids has been studied for decades, but there are still some issues that are still ripe for investigation, such as the mass loss mechanism (e.g. Neilson & Lester 2008; Neilson et al. 2016), the mass discrepancy between pulsation and evolution models (e.g. Keller 2008; Neilson et al. 2011), or the multiplicity fraction (e.g. Evans 1995; Evans et al. 2005, noting that here we use 'binary' as shorthand for 'binary or multiple'). Binary Cepheids offer the possibility to probe several aspects, such as the Cepheid evolution or the determination of the Cepheid mass.

More than 50% of intermediate mass main sequence stars, which are the progenitors of Cepheids, are in binary systems (Duchêne & Kraus 2013). Therefore, we expect a similar probability for Cepheids; however, the binary fraction of Cepheid seems lower than expected. However, population synthesis models suggest that the binary fraction of Cepheids should be significantly less than that of their progenitors due to binary interaction in the red giant branch phase (Neilson et al. 2015). In addition, Evans et al. (2005) noted that about 35% of the Galactic Cepheids have a spectroscopic companion (see also Shetye et al. 2024) and 44% of those being in a multiple system. This would correspond to a spectroscopic binary fraction of those intermediate mass main sequence progenitors of ∼40–45% (Neilson et al. 2015). However, this low binary fraction is due to incompleteness. Recent work of Kervella et al. (2019c,b, 2022) combined the HIPPARCOS and *Gaia* DR2 positions to determine the mean proper motion of nearby classical Cepheids and derived a binary fraction of >80%. This is significantly higher than the predicted (Neilson et al. 2015) and the

⋆ Corresponding author: agallenne@academicos.uta.cl

observed values: 32−52% from Anderson et al. (2016), 40−70% for their Milky Way progenitors from Chini et al. (2012) and ∼50% for their progenitors in the cluster Scorpius OB2 from Kouwenhoven et al. (2005). We note that eight of the nine nearest classical Cepheids within 500 pc are members of binary systems and that they host, on average, more than one companion (Kervella et al. 2019b). The only object not yet established as a binary is ζ Gem, although it does have a visual companion.

Binary statistics are fraught with selection effect due to the observing techniques used to detect the companions, either because they cannot reach a high dynamic range, the angular resolution is limited, or they cannot detect small orbital motions from radial velocities. Detecting the companions is a challenging task because of the brightness of the Cepheid and close components are hardly detectable from imaging. Most of the binary Cepheids were detected from radial velocities and are single-line spectroscopic binaries (see e.g. Lloyd Evans 1982; Welch et al. 1987; Evans 1988; Szabados 1991; Evans 1994; Szabados & Nehéz 2012; Evans et al. 2013; Szabados et al. 2013; Evans et al. 2015; Pilecki et al. 2015; Anderson et al. 2016; Pilecki et al. 2018; Gallenne et al. 2019; Shetye et al. 2024; Hocdé et al. 2024). From spectroscopic observations, we can detect the orbital motion of the Cepheid if the companion is close and massive enough to produce a detectable effect in the radial velocities. Detection of the companion's spectral lines is difficult because most of the known companions are hot main sequence stars with broad and blended lines. Ultraviolet (UV) spectroscopy has proven to be efficient in detecting the hottest companions and characterising their spectral types and temperatures from low- and high-resolution spectra obtained with the International Ultraviolet Explorer (IUE) and Hubble Space Telescope (HST) satellites (see e.g. Evans 1992a; Massa & Evans 2008). Combined with a mass-temperature relation, the companion mass can be inferred. High-resolution UV spectra also make possible the detection of spectral lines for a few companions and the measurements of their radial velocities. When taken at maximum and minimum orbital velocities, the velocity amplitude of the companion combined with the orbital velocity amplitude of the Cepheid determined from the ground and the inferred mass of the companion provides an estimate of the Cepheid mass (see e.g. Böhm-Vitense et al. 1997; Evans et al. 1998, 2011, 2018b). Radial velocity measurements are the easiest and most frequently applied method to identify and characterise binary Cepheids (Evans et al. 2015).

Dynamical mass determinations (and, hence, model-independent determinations) requires astrometric measurements of the companion's orbit, in addition to the spectroscopic orbit and an assumed distance to the Cepheid. However, this is a challenging task due to small separations ($\lesssim$50 mas) and contrast ($\gtrsim$3 mag in H). The first dynamical mass was measured by Evans et al. (2008) who spatially resolved the spectroscopic companion of Polaris located at ∼170 mas using the High Resolution Channel (HRC) of the Advanced Camera for Surveys (ACS) on board HST. Follow-up observations provided a mass precise to ∼20% (Evans et al. 2018a). New observing techniques such as near-infrared (NIR) long-baseline interferometry have strong potential for spatially resolving binary Cepheids (see e.g. Gallenne et al. 2013). Gallenne et al. (2018) combined astrometric measurements from interferometry with ground-based radial velocities of the Cepheid and space-based radial velocities (HST/STIS) of the companion. They measured the most precise mass for a Galactic Cepheid (V1334 Cyg, 3%) and its companion (1%), together with the most precise distance for a Cepheid (1%). Other binary Cepheid systems are also promising for precisely measuring their masses and distances (Gallenne et al. 2019, 2015, 2014b).

Wider separations were explored for 70 bright Cepheids using the HST and its Wide Field Camera 3 (WFC3; Evans et al. 2020, 2016, 2013). Several companions were detected in the range 0.5″−5″ for 13 Cepheids. Their colour-magnitude diagram showed that the companion masses are evenly distributed, although a bias is expected at small separations as low-mass stars are more difficult to detect. In addition, the HST point-spread-function (PSF) within 2″ is complicated and required sophisticated image processing. Interestingly, all detected companions within 2″ are themselves spectroscopic binaries. Evans et al. (2020) suggested that the wider companion is likely formed first, followed by the formation of the inner spectroscopic binary through disk fragmentation. Gallenne et al. (2014a) also investigated the presence of visual companions around five Cepheids using adaptive optics (AO) imaging with the VLT/NACO instrument, detecting a companion only for η Aql.

In this paper, we want to explore the Cepheid duplicity using high-contrast imaging to detect faint and nearby orbiting companions. We probe the spatial scale 0.02″−3.5″ in three different photometric filters with the SPHERE instrument. This paper is organised as follows. In Sect. 2, we present the observations and data reduction. We then describe our data analysis in Sect. 3, including the method we used to search for companions, the position and flux estimates, and the detection limits for undetected components. We discuss the results in Sect. 4 and the conclusions in Sect. 5.

2. Observations and data reduction

We observed 47 Galactic Cepheids with the extreme adaptive optics instrument SPHERE (Spectro-Polarimetric High-contrast Exoplanet REsearch; Beuzit et al. 2019), corresponding too all observable Cepheids with $V < 8$ mag to have the best AO performances. Data were acquired in 2018 and 2020 with the ZIMPOL instrument (Schmid et al. 2017, 2018) in classical imaging mode (i.e. without coronagraph) in the optical. Observations were taken in pupil-stabilised mode to obtain the best PSF stability. ZIMPOL is a two-arm imager with two CCD detectors, which enabled us to acquire quasi-simultaneous observations in two different filters. The field of view of each detector is 3.5″ × 3.5″. As the identified companion of Cepheids are mostly hot main sequence stars (Evans et al. 2022), our observing strategy was to obtain images in the V band in one arm and in two red filters (R' and I') on the second arm. This combination of filters should allow us to determine the spectral type of the detected companions. The full log of our observations is listed in Table A.1. Each observation include three dithering positions to remove artefacts such as bad pixels, cosmic rays, or fixed pattern noise.

To save observing time, no photometric calibrators were observed. In addition, the brightest Cepheids saturated the detectors so that a neutral density filter had to be used. Therefore, in this work, we can only estimate V, R', and I' flux ratios between the detected companion and the Cepheid, $f = f_{\rm comp}/f_{\rm ceph}$.

The data reduction of ZIMPOL images was carried out by the High-Contrast Data Center (Delorme et al. 2017; Beuzit et al. 2019)[1] using an implementation of the SPHERE-ZIMPOL software package described in Schmid et al. (2017). It includes standard procedures such as dark, flat, and bad pixel correction. Individual frames were also de-dithered and re-aligned so that

[1] https://hc-dc.cnrs.fr

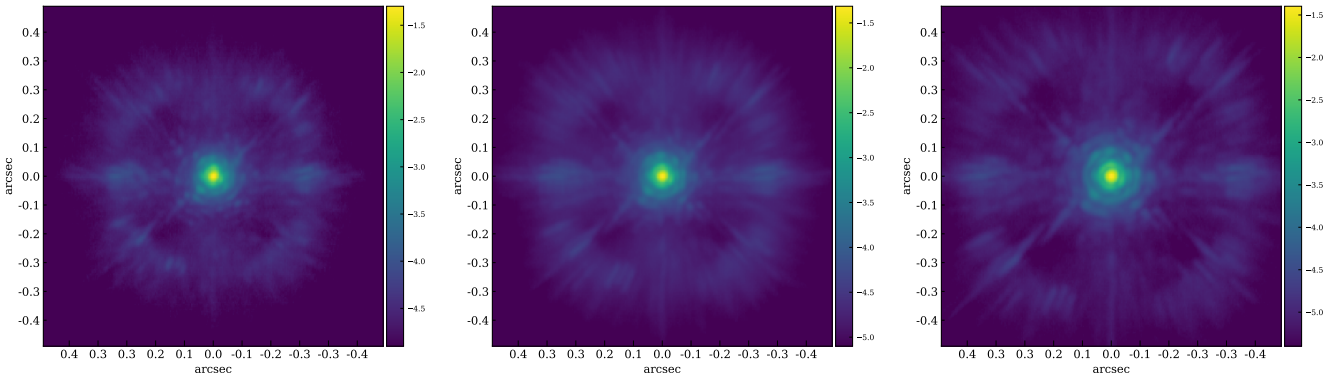

Fig. 1. Average images of FF Aql in V (left), R' (middle) and I' band. The scale is logarithmic and the images have been cropped to $1'' \times 1''$ to better see the PSF quality.

the final output of the data reduction consists in a single non de-rotated cube for each filter. Most of the observations were obtained under very good seeing conditions (average seeing of $0.73''$; see Table A.1), so that each frame in a cube has a good point spread function (PSF). The worst conditions were for the Cepheid V659 Cen, with an average seeing of ∼1.5. To present the quality of the PSFs, we display as examples in Fig. 1 the cube-averaged images of FF Aql in V, R', and I' bands, where several Airy rings are visible, even in V.

3. Data analysis

3.1. Searching for companions

To search for companions around our Cepheid sample, we modelled and subtracted the PSF using a principal component analysis (PCA; Amara & Quanz 2012) implemented in the Vortex Image Processing library, which is a `python` package dedicated to high-contrast imaging (VIP; Gomez Gonzalez et al. 2017)[2]. We chose the PCA approach instead of other post-processing algorithms (e.g. locally optimised combination of images, LOCI, Lafrenière et al. 2007, non-negative matrix factorisation, NMF, Lee & Seung 1999, or local low-rank plus sparse plus Gaussian-noise decomposition, LLSG, Gomez Gonzalez et al. 2016) because of its good performance and processing speed. A PCA uses all images in a given data cube to model the variation of the PSF in time by identifying the principal linear components (PCs). The number of PCs determines how well the PSF is fitted, with the first components containing the most common structures. An image is built from these first components and then subtracted from the images to remove the speckle pattern. This image processing method is commonly used for exoplanet direct detection and is usually combined with additional post-processing techniques, such as angular differential imaging (ADI; Marois et al. 2006) or reference star differential imaging (RDI; Lafrenière et al. 2009; Soummer et al. 2011; Gerard & Marois 2016).

Our observations were carried out in pupil tracking mode, which we expected would allow us to apply the ADI technique. However, the observing sequences have too short an exposure time, so the variation of the parallactic angle (PA) in the cube ends up too small, possibly leading to self-subtracted companions (especially the closest ones). We therefore chose to test three different approaches of PCA-based ADI techniques to detect the companions. The first one (#1) consisted of only taking the first and last 12 frames of the data cubes. For the second approach (#2), we rotated the frame, i, of the cube by an additional angle of 0.5°, so that the PA of the frame i has $+i * 0.5°$ (first frame having $i = 0$). We refer to this as a fake ADI. The last approach (#3) is also a fake ADI but combined with a RDI-like method, namely, we rotated the second half of the cube by +180° and took the first half as a reference. Each approach uses one principal component because we noticed that larger values did not necessarily provide a better detection and tended, rather, to remove the closest companions. In addition, this is a pre-analysis whose goal is to identify a possible companion and obtain its approximate location.

To test which approach would be better in detecting companions, we took one of our SPHERE data cubes for which there is no visible bright companions (FF Aql in band I') and we injected fake companions at $0.1''$, $0.2''$, $0.5''$, $1.0''$, and $1.5''$ from the central star and at an angle of 185.4°. It corresponds to the mean parallactic angle of the cube and where we see the brightest speckle pattern within $0.5''$ (most pessimistic case for sensitivity). All the injected companions had the same flux ratio, $f_{\rm comp}/f_\star = f = 0.1\%$, in an aperture where the full width at half maximum (FWHM) of the PSF was estimated by taking the median of the original data cube (i.e. no companions injected). Thus, we obtained an aperture of $1 \times$ FWHM. We used the functionalities included in the `VIP` package for that purpose. The data cube quality is very good, with a FWHM of 22.6 mas, close to the theoretical diffraction limit of ∼20 mas in V. We display the image with injected companions in Fig. 2.

For each approach, we estimated the estimated the signal-to-noise ratio (S/N) in a resolution element at the expected positions of the companions. We used the `snr` module of the `VIP` package which implements the approach described in Mawet et al. (2014) where a penalty term is applied to the S/N to account for the small sample statistics at small separations from the central star. Each companion location was tested against the background resolution elements at the same radial distance from the centre. We defined a detection threshold of S/N > 5 above the background level[3] (chosen as being the median background of the image plus 5σ). Finally, we repeated the entire process, this time with higher contrast companions of $f = 0.02\%$. We display the PCA-ADI results in Fig. 3 for both flux ratios and the detec-

[2] https://github.com/vortex-exoplanet/VIP

[3] S/N is not the Gaussian significance, i.e. not the confidence level of a Gaussian $n\sigma$. S/N can be converted to $n\sigma$, however, values are similar for S/N $\lesssim 8$, while computer precision limits the conversion to higher S/N values.

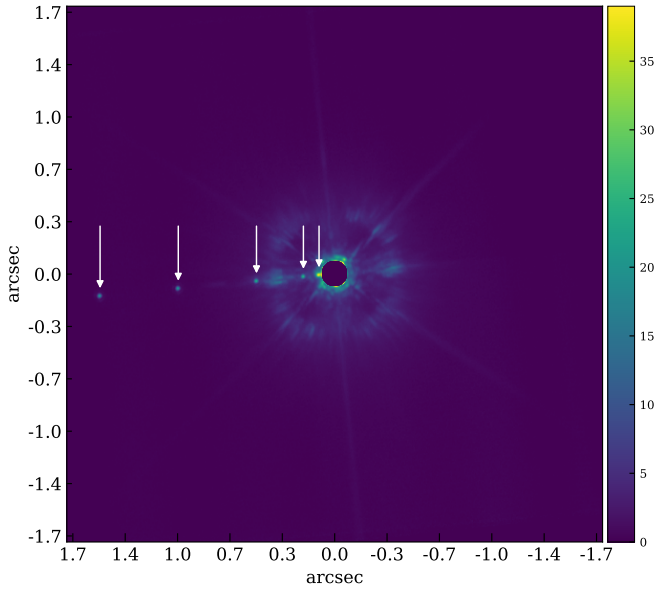

Fig. 2. De-rotated average image of FF Aql in the I' band, where we injected five fake companions (indicated with arrows). A fake central mask is inserted for the display purposes.

tion levels $n\sigma$ of each companion for all approaches are listed in Table 1.

As expected, the closest companion is not significantly detected (i.e. $\sigma < 5$) for any approaches, as well as the second companion at higher contrast. Between all approaches, #2 offers the best detection level at any separations. Approach #3 seems to be better than #1 for small separations; however, the residual noise is larger in the central part. To perform a cross-check for possible detections, we chose to search for companions using the three approaches across our full dataset. When a companion was identified, we applied a PCA on a single annulus with the true parallactic angles (width of $3 \times$FWHM) encompassing the companion candidate. We optimised the S/N at its position by searching for an optimal number of PCs. The S/N and significance level for all detected companions are listed in Table 2.

We detected companions with $S/N > 5$ for only 8 Cepheids (i.e. 17% of our sample). The PCA-ADI frames with the detected companion are displayed in Fig. 4. The fluxes and astrometry are determined in the next section. When no companions were detected, we estimated the detection limits according to the procedure explained in the following section.

3.2. Position and flux estimate of detected companions

We applied the method available in `VIP` using the negative fake companion technique (NEGFC; Lagrange et al. 2010; Marois et al. 2010) for the determination of the flux and position of the companion, coupled with Monte Carlo methods to estimate uncertainties. Briefly, the NEGFC technique consists of injecting a negative fake companion into the raw data cube with flux and position close to the expected values, performing a PCA on an annulus passing through the expected companion position and extracting the flux on a circular aperture centred at the position of the companion (chosen as three times the FWHM of the PSF). In our study, these steps were iteratively repeated to minimise the total flux within the circular aperture, with the companion parameters defined by the `emcee` affine invariant algorithm (Foreman-Mackey et al. 2013) at each iteration. The astrometric positions are reported in Table 3, where we took the mean value between the three filters and the corresponding standard deviation as uncertainty. However, due to the limited field rotation in our images, self-subtraction may lead to an underestimation of the flux. To obtain a more accurate flux measurement, we performed the aperture photometry for both the Cepheids and their companions using the median image of the de-rotated cube. The resulting flux ratios between the companions and the Cepheids are also presented in Table 3. Finally, position angles were corrected for the ZIMPOL true north offset of $-2°$ (Schmid et al. 2017, 2018; Engler et al. 2018).

3.3. Detection limits

For Cepheids where no companions were detected, we employed the `VIP` `contrast_curve` function to produce contrast curves by injecting synthetic companions, assessing noise and throughput following PCA-based PSF subtraction, and determining the 5σ detectable flux ratio as a function of separation. A Student-t correction, as outlined by Mawet et al. (2014), was applied to account for small-sample statistics. In Fig. 5, we display the contrast curve for eight Cepheids.

4. Discussion

In our sample, 41 out of 46 Cepheids (89%) are confirmed binary or triple systems (Szabados 2003), with one additional Cepheid, BQ Ser, considered a suspected binary (Gorynya et al. 1996). This aligns with the works from Kervella et al. (2019c), where we estimated a binary fraction exceeding 80% by analysing proper motion anomalies using combined HIPPARCOS and *Gaia* DR2 positional data. However, in this study, we only identify a companion for eight of these Cepheids, indicating that the majority of them are likely spectroscopic binaries.

Three Cepheids have a visual companion, according to Szabados (2003): V339 Cen, AX Cir and RY Sco. In the case of V339 Cen, no evidence of a companion is found in the existing literature, whether through spectroscopy or astrometry (Kervella et al. 2019a). Furthermore, our observations similarly show no visual component within 1.7″. AX Cir forms a triple system, exhibiting both a spectroscopic companion (e.g. Petterson et al. 2004; Gallenne et al. 2014b) and a visual companion (Evans et al. 2020), with the latter's wider component having been confirmed by our SPHERE observations. For RY Sco, its visual companion, positioned at ∼2.2″ from the Cepheid, falls outside our field of view (FoV).

Additional candidate visual companions for V496 Aql, V350 Sgr, BB Sgr, and RV Sco, which are not mentioned in Szabados (2003), were identified by Evans et al. (2020). However, these are situated beyond 2″ from the Cepheid, placing them outside our FoV. Evans et al. (2020) also reported visual companions within 2″ for S Nor, η Aql, and AX Cir, which we confirm in this study. We also report the new discovery of a wide companion associated with the Cepheids AP Pup, T Vel, and TX Del.

The probability that any of the detected companions is a chance alignment with a field star is expected be low given the small FoV of our observations (∼3.5″). To quantify this, we queried the *Gaia* DR3 catalogue for sources brighter than $G = 18$ mag within a radius of 50″ around each Cepheid hosting a detected companion and used the resulting counts to estimate the local surface density of field stars. Assuming Poisson statistics, we converted this density into the probability of finding at

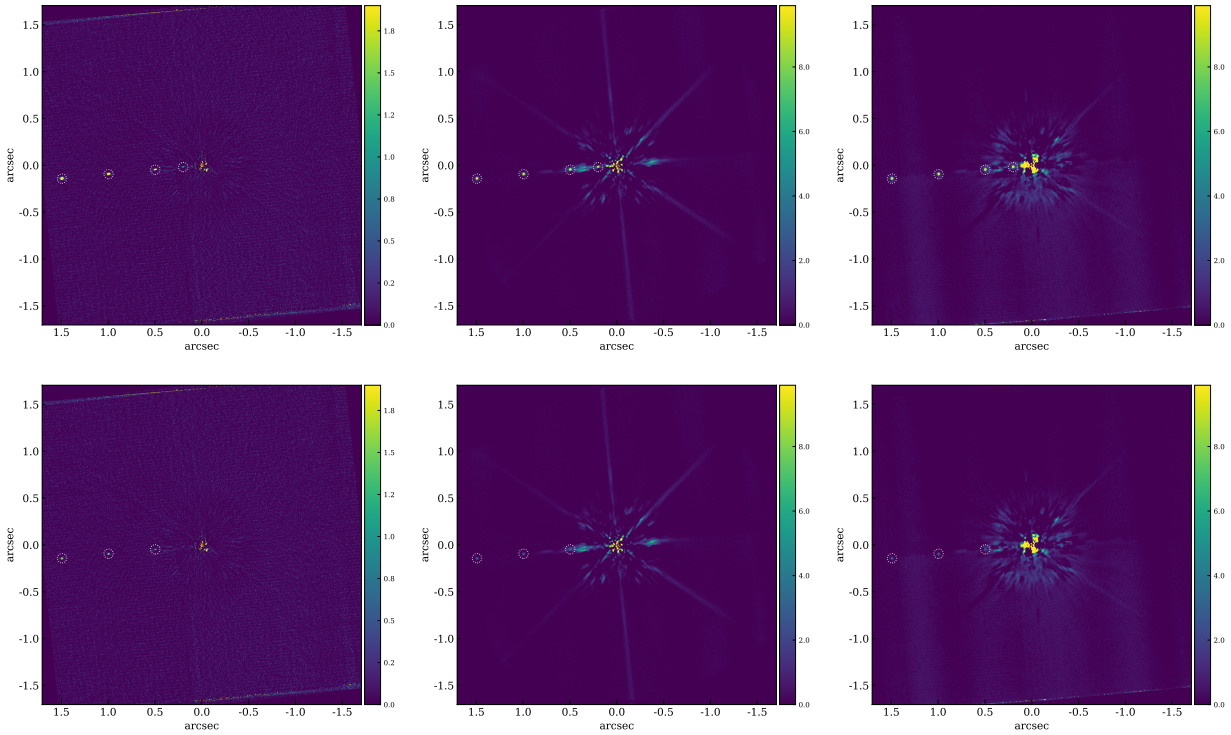

Fig. 3. *Top*: Full-frame PCA-ADI results for the three ADI approaches (#1, #2, #3) with injected companions of flux ratio of 0.1%. *Bottom*: Same as above but with flux ratio of 0.02%. The companions with S/N > 5 are circled.

Table 1. Detection level ($n\sigma$) of the injected companions for our three PCA-ADI approaches and two different flux ratios.

	S/N f = 0.1%			S/N f = 0.02%		
	#1	#2	#3	#1	#2	#3
#1 (0.1″)	1.2	3.9	3.2	0.2	2.2	2.1
#2 (0.2″)	7.7	8.2	6.2	3.7	4.3	2.9
#3 (0.5″)	>8.2	>8.2	>8.2	>8.2	8.1	5.1
#4 (1.0″)	>8.2	>8.2	>8.2	>8.2	>8.2	>8.2
#5 (1.5″)	>8.2	>8.2	>8.2	>8.2	>8.2	>8.2

Table 2. S/N of the detected companions around our Cepheids in all filters with the annular PCA analysis.

	S/N		
	V	R'	I'
η Aql	39.5	55.3	16.1
V659-Cen	–	33.5	44.1
AX Cir	18.9	21.8	16.2
TX Del	28.7	26.1	23.6
S Nor	35.3	28.9	18.6
AP Pup	11.9	14.4	25.0
W Sgr	79.0	45.9	15.2
T Vel	48.7	33.1	37.1

least one field star within a radius of 1″ (i.e. the region encompassing all of our detected companions). For η Aql, for example, we found 12 stars, corresponding to a density of 0.0015 arcsec^{-2}, which implies a probability <0.5% that the detected companion is an unrelated field star. For the remaining Cepheids, the corresponding probabilities are <2%, with the exception of W Sgr, for which we obtain ∼6%. However, when evaluated at the measured separation of the companion (0.2″), the probability that the detected companion is a field star physically unrelated to the Cepheid decreases to ∼0.2%.

4.1. Detected companions

In this section, we explore the companions we identified and provide additional details regarding their specific characteristics. Unfortunately, performing absolute photometry was not possible due to the lack of photometric zero-point data for our filter bandpasses, which would only allow for the measurement of flux ratios between the Cepheid and its companion. However, the Cepheid's magnitude at a specific phase can be estimated using the Berdnikov (2008) light curves, available in standard Johnson-Cousins filters. Although the transmission profiles of these filters differ slightly from those of SPHERE, they are sufficiently similar for practical use. By integrating stellar atmosphere models over the filter bandpasses across various temperature ranges, we determined a maximum magnitude difference of 0.13 mag at the lowest temperature (4500 K), which decreases with increasing temperature. Consequently, to estimate the companion's magnitude, we utilised the measured flux ratios combined with the expected Cepheid magnitude at the corresponding pulsation phase[4], as derived from the Berdnikov light curves, adopting an uncertainty of 0.1 mag.

To estimate the de-reddened magnitudes, we adopted the reddening law of Fouqué et al. (2007), i.e. $R_V = 3.23$, $A_V = R_V E(B-V)$, $A_{R_C} = 0.645 A_V$ and $A_{I_C} = 0.608 A_V$. All uncertainties were propagated til the final results. The phases

[4] Estimated from a spline interpolation.

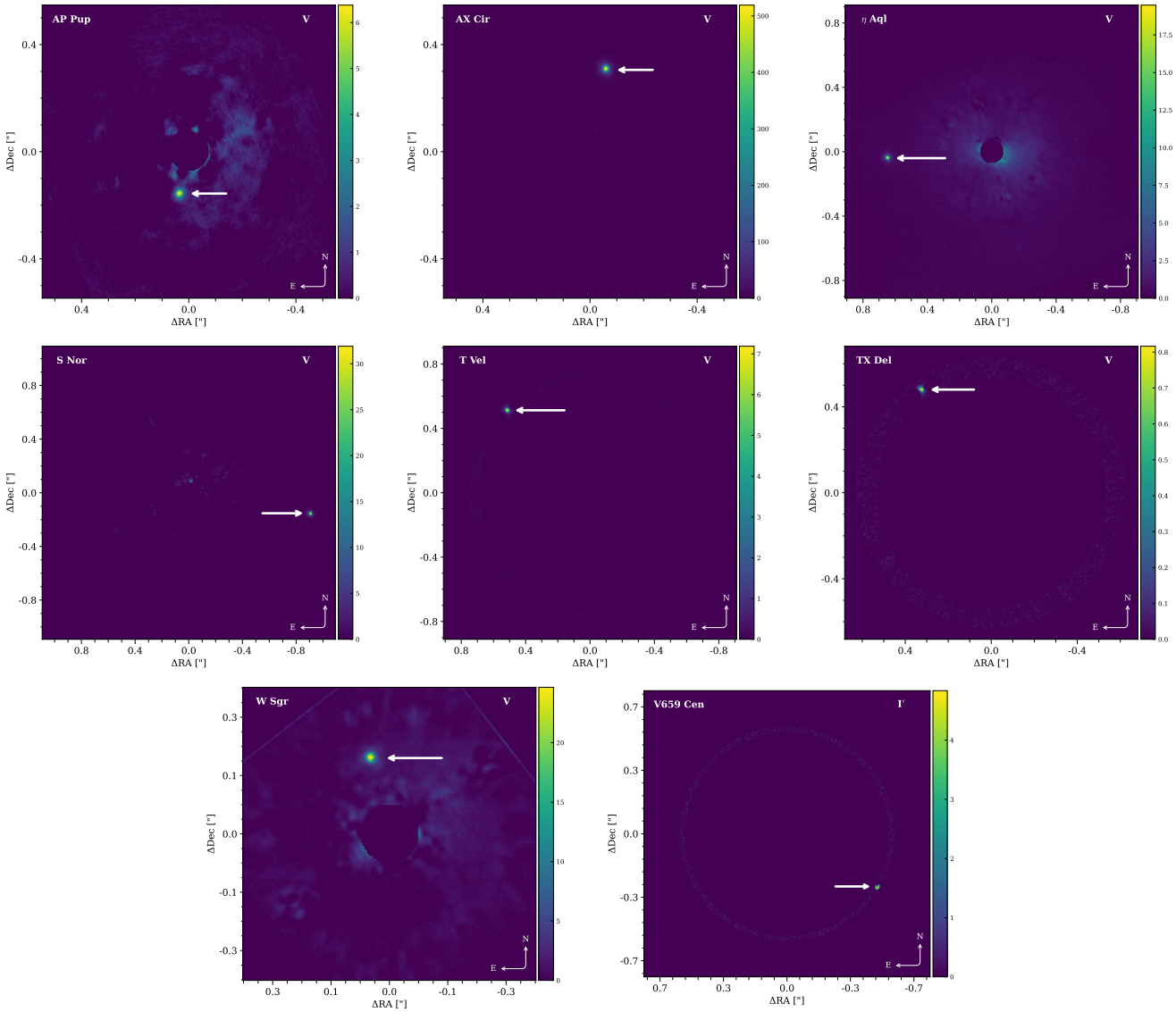

Fig. 4. PCA analysis of our Cepheids with detected companion in V, except for V659 Cen, which is in I' (see text).

at our observing epoch were calculated using the ephemeris from Csörnyei et al. (2022), and propagating the rate of pulsation change for η Aql, AX Cir, AP Pup, W Sgr, and T Vel. For TX Del, we used the ephemeris from *Gaia* DR3 and the rate of period change from Percy & Hoss (2000), and from (Trahin et al. 2021) for S Nor.

η Aql: The wide companion of this Cepheid was already reported, and our observations of the companion's position align with those reported by Evans et al. (2020) and Gallenne et al. (2014a). The companion exhibited a positional shift of 4.1° between the initial and final epochs. Assuming a circular, face-on orbit, this translates to an angular velocity of approximately $0.546°\,\mathrm{yr}^{-1}$, suggesting a minimum orbital period of about 659 yr.

From the light curves, the Cepheid magnitude at the pulsation phase 0.61 is $V = 3.9 \pm 0.1$ mag, $R' = 3.4 \pm 0.1$ mag and $I' = 3.0 \pm 0.1$ mag (prime indices are omitted for simplicity and clarity). With a colour excess $E(B-V) = 0.16 \pm 0.02$ (Trahin et al. 2021) and our flux ratios, we calculated the companion's de-reddened magnitudes $V_0 = 9.4 \pm 0.2$ mag, $R'_0 = 9.1 \pm 0.1$ mag and $I'_0 = 9.0 \pm 0.1$ mag. To compute the absolute magnitudes, an accurate distance to this bright star is required. Distance estimates from *Gaia* (270 ± 14 pc[5]), Kervella et al. (2004, 276 ± 55 pc) or Gieren et al. (2018, 252 ± 27 pc) are mutually consistent, providing a reliable accuracy. We adopted a mean distance of $d = 266 \pm 10$ pc calculated from these sources. This results in absolute magnitudes of $M_V = 2.2 \pm 0.2$ mag, $M_{R'} = 1.9 \pm 0.1$ mag, and $M_{I'} = 1.8 \pm 0.1$ mag. Assuming the companion is a main sequence star and using the spectral type calibration from Pecaut & Mamajek (2013), it would be classified between a A5V and a F3V star with a mass within $1.4-1.9\,M_\odot$. This is in agreement with our previous works using VLT/NACO (Gallenne et al. 2014a). This seems to also confirm the existence of a closer hotter companion, detected in an IUE spectrum, with a spectral type of B9.8V (Evans 1991). We will discuss this specific case in another publication combining different observing techniques (Gallenne et al., in prep.).

[5] All parallaxes were corrected from the parallax offset (Lindegren et al. 2021).

Table 3. Position and flux ratios of the detected companions.

	ρ (mas)	θ (°)	f_V (%)	$f_{R'}$ (%)	$f_{I'}$ (%)	Sp. Type
η Aql	639.4 ± 0.3	91.57 ± 0.09	0.42 ± 0.06	0.41 ± 0.01	0.32 ± 0.01	A5V-F3V
V659 Cen	597.3 ± 1.1	238.3 ± 0.4	–	–	–	–
AX Cir	309.9 ± 0.3	368.6 ± 0.1	7.2 ± 0.1	6.12 ± 0.02	4.58 ± 0.02	B6V
TX Del	573.8 ± 0.9	32.2 ± 0.4	0.007 ± 0.002	0.011 ± 0.002	0.015 ± 0.001	M0V-M1V
S Nor	907.3 ± 0.9	258.3 ± 0.4	0.275 ± 0.007	0.247 ± 0.004	0.236 ± 0.004	A3V-A4V
AP Pup	159.3 ± 0.2	165.0 ± 0.4	0.048 ± 0.003	0.053 ± 0.009	0.073 ± 0.012	F9V-G2V
W Sgr	192.1 ± 1.0	12.3 ± 0.5	0.284 ± 0.013	0.262 ± 0.007	0.241 ± 0.007	F0V-F2V
T Vel	716.5 ± 0.8	43.2 ± 0.4	0.022 ± 0.003	0.025 ± 0.005	0.027 ± 0.004	K2-K3V

Notes. ρ and θ are the relative separation of the companion w.r.t. the Cepheid and its position angle, while f_X denotes the measured flux ratio at band X. Sp. Type is our derived spectral type based on the flux ratio (see Sect. 4.1).

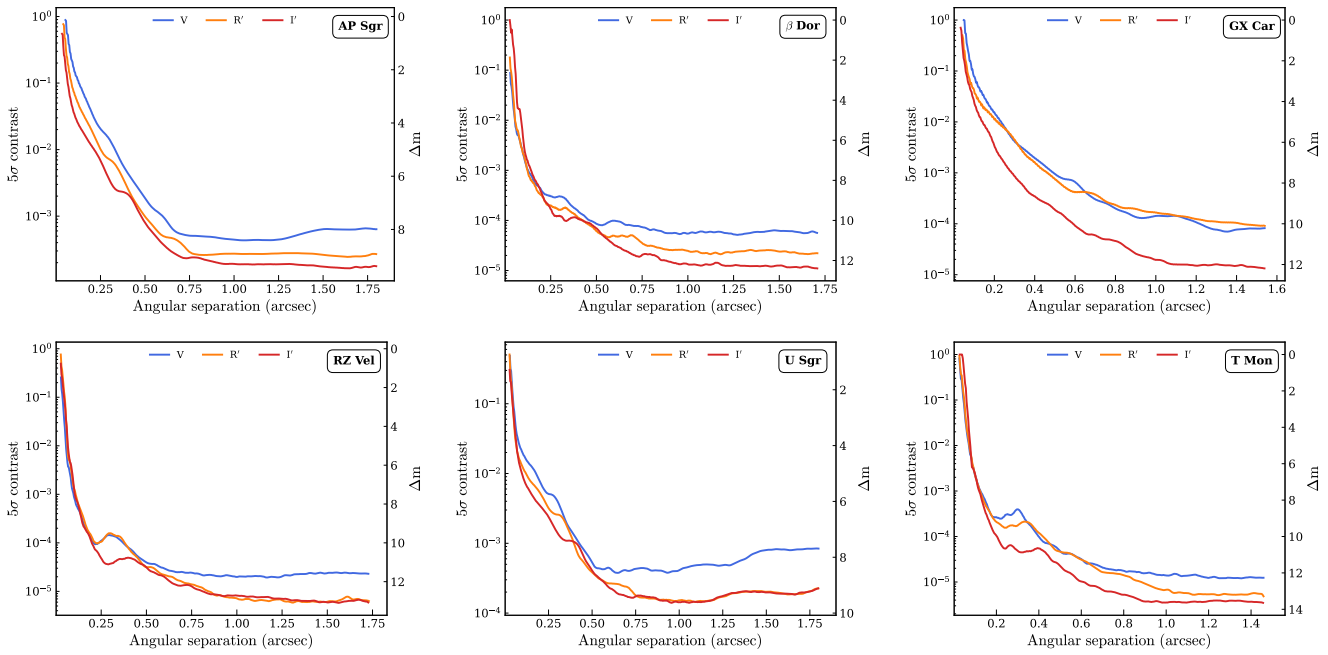

Fig. 5. 5σ contrast curves of six Cepheids of our sample with no wide companion detected.

V659 Cen: This star is member of a triple system comprising a spectroscopic binary and a wider component. Evans et al. (2020) reported an approximate separation of 0.6″ and a position angle of ∼235° for the wide companion using HST/WFC3 observations. Unfortunately, our SPHERE observations were hampered by poor observing conditions and sub-optimal adaptive optics corrections, preventing detection of the wide component in the V band due to insufficient flux. However, in the R' and I' filters, we obtained sufficient flux to accurately measure the companion's astrometric positions; however it was not high enough for accurate photometry. Our measurement is in very good agreement with Evans et al. (2020) and with the most recent position we determined in Evans et al. (2025, $\rho \sim 0.590''$ and PA = 237.8°) from the HST/STIS acquisition exposure. Assuming a circular orbit with low inclination, we estimated a minimum orbital period of approximately 749 years based on the angular velocity between 2011 (HST) and 2018 (SPHERE).

AX Cir: This complex system comprises at least three components. The spectroscopic component was spatially resolved through long-baseline interferometry (Gallenne et al. 2014b), yielding a semi-major axis of approximately 27 mas and an orbital inclination of about ∼55° (Gallenne et al., in prep.). The H-band interferometric flux ratio indicates a B9V star. A preliminary analysis of the companion's velocity from the STIS spectrum suggests it may itself be a binary. Additionally, a wide companion at approximately 0.3″ was detected via speckle interferometry (Tokovinin et al. 2019, $\rho = 0.313''$ and PA = 346.9°) and HST imaging (Evans et al. 2020, $\rho = 0.3''$ and PA = 332.4°). This component is the hottest one in the system and corresponds to the B6V star previously detected from IUE spectrum (Evans 1994). Our SPHERE astrometry aligns well with these prior measurements and confirms orbital motion. The observed angular velocity of 5.1° yr^{-1} between the HST observations (2011) and ours (2018) suggests a minimum orbital period of approximately 70 years.

Using the Cepheid light curves, we derived companion magnitudes of $V = 9.0 \pm 0.1$ mag, $R' = 8.6 \pm 0.1$ mag and $I' = 8.5 \pm 0.1$ mag. Adopting a colour excess of $E(B-V) = 0.31 \pm 0.01$ (Trahin 2019) and a *Gaia* distance $d = 505 \pm 63$ pc, we calculated absolute magnitudes of $M_V = -0.6 \pm 0.3$ mag, $M_{R'} = -0.6 \pm 0.3$ mag and $M_{I'} = -0.7 \pm 0.3$ mag. These values are consistent with the B6V spectral type reported by Evans (1994).

TX Del: This star is classified as a type II Cepheid (Harris 1981; Balog & Vinko 1995; Laney 1995) and has been reported to be a spectroscopic binary (Harris & Welch 1989). The large re-normalised unit weight error (RUWE) parameter of *Gaia* (Gaia Collaboration 2018) and the proper motion anomaly (Kervella et al. 2019a) confirm its binary nature. Harris & Welch (1989) published the orbital elements, with a period of 133 days. Adopting the *Gaia* distance of 1102 pc, a mass of 3.5 $M_\odot$ for the Cepheid (Kervella et al. 2019a) and assuming at most an equal mass for the companion, the maximum angular separation would be ∼0.9 mas. This is well below the spatial resolution of SPHERE.

Here, we report the astrometric detection of a third companion at an angular separation of 574 mas. Assuming the same mass for the companion as the Cepheid, this would provide from the Kepler law an approximate orbital period of 6000 years. From the light curves of Berdnikov and our measured flux ratios, we calculated apparent magnitudes of $V = 19.4 \pm 0.3$ mag, $R' = 18.3 \pm 0.2$ mag, and $I' = 18.2 \pm 0.2$ mag. Adopting a colour excess of $E(B-V) = 0.06 \pm 0.02$ (Lallement et al. 2018) and the *Gaia* distance, we calculated the absolute magnitudes of $M_V = 9.0 \pm 0.3$ mag, $M_{R'} = 7.9 \pm 0.2$ mag and $M_{I'} = 7.9 \pm 0.2$ mag. This would correspond to a M0-M1V companion.

S Nor: This Cepheid is known to have a confirmed wide, resolved companion and there is a possible close-in spectroscopic companion. Szabados (1989) reported evidence of an inner companion, but orbital motion remains largely undetected. Recent high-precision radial velocity measurements (Shetye et al. 2024; Gallenne et al. 2019) show no significant variations in systemic velocity, casting doubt on the presence of this close-in companion. Additionally, interferometric observations by Gallenne et al. (2019) detected no companion brighter than a B7V star within 50 mas. The wide companion, located at ∼0.9″, has been detected both spectrally and spatially. Evans (1992b) identified a B9.5V companion through an IUE spectrum, consistent with the photometric detection reported by Evans et al. (2020). We calculated a very small angular motion of ∼0.12° between our 2018 measurement and the HST (2011), suggesting a minimum orbital period of about 2951 years.

We estimated apparent magnitudes of $V = 12.5 \pm 0.1$ mag, $R' = 12.2 \pm 0.1$ mag and $I' = 11.8 \pm 0.1$ mag. Adopting $E(B-V) = 0.29 \pm 0.02$ (Trahin et al. 2021) and the *Gaia* distance of 910 ± 18 pc, we computed absolute magnitudes of $M_V = 1.8 \pm 0.1$ mag, $M_{R'} = 1.8 \pm 0.1$ mag and $M_{I'} = 1.4 \pm 0.2$ mag. This would correspond to a A3V star, which is slightly colder than the B9.5V estimate from Evans (1992b). A more accurate determination of the spectral type will require multi-wavelength observations.

AP Pup: This Cepheid is considered a potential spectroscopic binary based on orbital motion evidence noted by Szabados (1989). The IUE spectrum of Evans (1992b) provided an upper limit spectral type of A3V. The imaging survey by Evans et al. (2020) failed to detect the companion, likely due to limited spatial resolution. However, Kervella et al. (2019c) identified a proper motion anomaly, indicating a close companion with a maximum separation of about 300 mas and an orbital period up to 3100 years. We confirm the detection of this companion. We derived apparent magnitudes of $V = 15.9 \pm 0.1$ mag, $R' = 15.3 \pm 0.2$ mag and $I' = 14.5 \pm 0.2$ mag. Using the *Gaia* distance of 1083 ± 23 pc and $E(B-V) = 0.355 \pm 0.02$ (Lallement et al. 2018), we estimated absolute magnitudes $M_V = 4.6 \pm 0.2$ mag, $M_{R'} = 4.4 \pm 0.2$ mag and $M_{I'} = 3.6 \pm 0.2$ mag. This would correspond to a spectral type in the range F9V-G2V.

W Sgr: Initially proposed as a spectroscopic binary by Jacobsen (1974), this Cepheid was later confirmed by Babel et al. (1989), who determined an orbital period of 1780 days and a high eccentricity of 0.52. Petterson et al. (2004) refined these parameters using more precise RV data, establishing a period of 1580 days and an eccentricity of 0.4. Benedict et al. (2007) detected the companion's astrometric motion using the HST Fine Guidance Sensor, deriving full orbital elements, including a semi-major axis of 12.9 mas. Evans et al. (2009) set a companion spectral type upper limit of F5V from HST/STIS observations. In Gallenne et al. (2019), we failed to detect the companion within 50 mas of the Cepheid using long-baseline interferometry, as the data were only sensitive to companions earlier than B8V. The companion's proximity prevents detection with VLT/SPHERE.

Morgan et al. (1978) identified a wider companion, initially mistaken for the spectroscopic companion, but its position at 0.116″ was inconsistent with the orbital period reported by Babel et al. (1989). This companion aligns with a hotter star detected by Bohm-Vitense (1985) using IUE spectra, with an estimated temperature of 9400 K, corresponding approximatively to an A1V spectral type. HST/STIS observations by Evans et al. (2009) confirmed this wide companion as the hotter component, with a spectral type of A0V, located at a separation of $\rho = 0.1645 \pm 0.0006$ and PA $= 210.0 \pm 0.5°$. This is the companion detected in our observations, which suggests (according to the angular motion) a minimum period of about 36 yr. Finally, Evans et al. (2016) also identified a possible third companion, located at 6.3″.

We calculated the apparent magnitudes for the second companion detected by SPHERE of $V = 11.4 \pm 0.1$ mag, $R' = 11.0 \pm 0.1$ mag and $I' = 10.7 \pm 0.1$ mag. Using the distance of 428 ± 11 pc, based on the mean and standard deviation between Benedict et al. (2007) and *Gaia* parallaxes, along with $E(B-V) = 0.15 \pm 0.02$ (Trahin et al. 2021), we estimated absolute magnitudes of $M_V = 2.8 \pm 0.1$ mag, $M_{R'} = 2.6 \pm 0.1$ mag, and $M_{I'} = 2.2 \pm 0.1$ mag, consistent with an F1V main sequence star. This is somewhat cooler than the A0-A1V classifications inferred from IUE and STIS spectroscopy. Given the different wavelength ranges and methods applied, small uncertainties in reddening, flux calibration, and contamination by the Cepheid can easily translate into shifts across several sub-classes, so we regard our estimate as broadly consistent with an early-type companion. We note also that this companion was not detected by Tokovinin et al. (2020) from speckle interferometry, who set a detection limit of $\Delta I \sim 2.9$ mag. This is well below the ∼6 mag expected to detect an A0V star. This also raises doubts about the detection about 45 years ago by Morgan et al. (1978) with the same technique.

T Vel: This short-period Cepheid has long been suspected of binarity based on slow systemic velocity shifts seen across multi-epoch radial-velocity campaigns. Early works have already flagged it as a possible spectroscopic binary with a red companion (Gieren 1985). No widely separated, hot UV-bright companion has been confirmed, pointing to a relatively close, faint companion instead. In the *Gaia* era, Kervella et al. (2019c) reported no significant proper motion anomaly at the *Gaia* DR2 epoch.

We report the detection of a relatively faint companion located at ∼717 mas from the Cepheid. We calculated its apparent magnitude of $V = 17.4 \pm 0.2$ mag and $I' = 16.0 \pm 0.2$ mag.

Table 4. 5σ contrasts and upper limits spectral type for undetected main sequence companions.

Star	0.25″		0.50″		>1″		Star	0.25″		0.50″		>1″	
	ΔV	SpT	ΔV	SpT	ΔV	SpT		ΔV	SpT	ΔV	SpT	ΔV	SpT
FF Aql	5.5	A3V	7.5	F6V	8.5	G2V	RV Sco	5.8	F0V	8.2	G4V	7.9	G1V
FN Aql	5.5	A3V	7.5	F6V	8.5	G2V	RY Sco	6.2	A3V	8.7	F8V	8.8	F9V
KL Aql	2.4	B1.5V	4.4	B7V	7.1	A9V	V482 Sco	6.5	F2V	9.4	K1V	10.0	K3V
V496 Aql	6.1	F0V	9.3	K0V	9.6	K1V	V636 Sco	5.9	A6V	8.7	G4V	9.6	K1V
V916 Aql	3.8	B3V	6.1	A0V	6.1	A1V	RU Sct	5.8	A0V	8.6	F7V	9.5	G2V
V1344 Aql	6.4	A9V	9.6	K0V	9.9	K1V	Y Sct	5.8	A3V	8.6	G0V	8.7	G1V
V340 Ara	8.5	F5V	10.1	G5V	10.8	G9V	S Sge	5.5	A3V	7.9	F9V	8.0	F9V
GX Car	5.3	F1V	7.5	G6V	10.0	K6V	BQ Ser	8.9	G9V	10.0	K3V	10.9	K6V
U Car	8.9	F5V	10.2	G1V	10.7	G7V	AP Sgr	4.2	A2V	6.8	F8V	8.2	G8V
UW Car	6.3	F1V	9.0	G9V	10.3	K4V	BB Sgr	5.3	A3V	7.9	F9.5V	7.7	F8V
V339 Cen	7.5	F5V	10.0	K0V	10.5	K3V	U Sgr	5.7	A7V	8.2	G2V	8.0	G0V
RZ CMa	5.1	A7V	8.3	G8V	8.6	K0V	V350 Sgr	6.3	A9V	9.2	G9V	9.9	K2V
β Dor	8.8	G3V	10.2	K2V	10.6	K3V	WZ Sgr	5.7	B9V	8.6	F4V	8.9	F5V
T Mon	8.8	F2V	10.8	G5V	12.2	K3V	X Sgr	5.5	A1V	8.2	F7V	8.4	F8V
TX Mon	4.7	B9.5V	7.0	F2V	7.0	F2V	Y Sgr	5.8	A3V	8.3	F9.5V	8.5	G0V
V465 Mon	6.2	A3V	8.8	G0V	10.4	K1V	YZ Sgr	6.1	A3V	9.2	G3V	9.9	G9V
BF Oph	5.5	A8V	8.1	G4V	7.6	F9.5V	LR Tra	5.1	A5V	7.9	G2V	8.0	G4V
Y Oph	6.1	B9.5V	9.2	F7V	9.3	F8V	R Tra	6.2	F3V	9.0	K1V	8.9	K0V
X Pup	4.6	B3V	7.1	A2V	8.5	F1V	RZ Vel	9.9	G7V	11.0	K3V	11.6	K4V
V Vel	6.1	A9V	9.0	G8V	9.8	K2V							

Berdnikov (2008) does not contain photometric measurements in R_C, we therefore interpolated the V and I_C band light curve at 700 nm to estimate $R' = 16.6 \pm 0.2$ mag. Using the *Gaia* distance of 1064 ± 18 pc and $E(B-V) = 0.29 \pm 0.02$ (Trahin 2019), we estimated the absolute magnitudes as $M_V = 6.3 \pm 0.2$ mag, $M_{R'} = 5.9 \pm 0.2$ mag, and $M_{I'} = 5.3 \pm 0.2$ mag. This would correspond to a K2-K3V companion.

4.2. Detection limits

For the remaining 39 Cepheids without a detected companion, we derived 5σ contrast limits for any unseen component, as described in Sect. 3.3. Examples of these contrast curves are shown in Fig. 5 and the limits at various separations are given in Table 4, together with the corresponding upper limits on the spectral type of an undetected main sequence companion. For the conversion, we also used the V-band light curves from Berdnikov (2008) and de-reddened the magnitudes with colour excesses from the literature (e.g. Csörnyei et al. 2022; Trahin et al. 2021; Groenewegen 2020; Trahin 2019; Turner 2016; Fernie et al. 1995). The upper limits on the companion spectral types were then obtained from the corrected *Gaia* parallaxes and the spectral-type calibration of Pecaut & Mamajek (2013), as in the previous sections.

We achieved maximum contrasts of approximately 10, 11, and 12 mag at separations of 0.25″, 0.50″, and >1″, respectively, while the mean contrasts over the whole sample are 6.1, 8.6, and 9.2 mag at these separations. For some Cepheids, at separations larger than 0.5″, we can exclude the presence of companions as late as K-type main sequence stars.

5. Conclusion

We present the first VLT/SPHERE survey of bright Galactic Cepheids, aimed at resolving faint visual companions on spatial scales between ~0.02″ and 3.5″. Using ZIMPOL imaging in the V, R', and I' bands, we obtained high-quality point-spread functions with a spatial resolution down to ~20 mas in V. Our observing strategy, combined with a PCA-based post-processing analysis, allowed us to measure accurate relative astrometry and flux ratios for detected companions and to derive stringent 5σ contrast curves for systems with no detections.

We detected visual companions around eight Cepheids (η Aql, V659 Cen, AX Cir, TX Del, S Nor, AP Pup, W Sgr, and T Vel), corresponding to about 17% of our sample. For η Aql, AX Cir, S Nor, W Sgr, and V659 Cen we confirmed previously known wide companions and refined their astrometric positions, providing new constraints on their long orbital periods. For AP Pup, T Vel, and TX Del we report the discovery of new wide companions with spectral types ranging from late F to mid-K on the main sequence. These systems highlight the wide range of configurations in which Cepheids are found.

For the remaining 39 Cepheids, we derived 5σ detection limits as a function of separation, reaching typical maximum contrasts of ~10, 11, and 12 mag at 0.25″, 0.50″, and >1″, respectively, with mean contrasts of 6.1, 8.6, and 9.2 mag across the sample. In several cases, we have been able to exclude, at separations beyond 0.5″, the presence of main sequence companions as late as K dwarfs. These limits demonstrate that most unresolved companions inferred from radial velocities and proper-motion anomalies must lie either at smaller separations than those probed here or at contrasts below our detection thresholds. Our SPHERE survey therefore provides a crucial high-contrast complement to spectroscopy, interferometry, and *Gaia* astrometry, helping to map the full multiplicity architecture of Galactic Cepheids. Finally, the improved sensitivity and contrast expected from the SPHERE+ upgrade (Boccaletti et al. 2020) will enable us to extend this type of survey to fainter Galactic Cepheids, further refining the census of their companions and multiplicity properties.

Acknowledgements. This work is based on observations collected at the European Southern Observatory under ESO programme 0101.A-0214. AG acknowledges the support of the Agencia Nacional de Investigación Científica y

Desarrollo (ANID) through the FONDECYT Regular grant 1241073 and ANID-ALMA fund No. ASTRO20-0059. PK, GP and WG acknowledge funding from the European Research Council (ERC) under the European Union's Horizon 2020 research and innovation program (project UniverScale, grant agreement 951549). GP acknowledges financial support from the Polish Ministry of Science and Higher Education with the grant agreement 2024/WK/02. GP and PK acknowledge support from the Polish-French Marie Skłodowska-Curie and Pierre Curie Science Prize awarded by the Foundation for Polish Science. B.P. acknowledges funding from the Polish National Science Center grant SONATA BIS 2020/38/E/ST9/00486. This work has made use of data from the European Space Agency (ESA) mission *Gaia* (https://www.cosmos.esa.int/gaia), processed by the *Gaia* Data Processing and Analysis Consortium (DPAC; https://www.cosmos.esa.int/web/gaia/dpac/consortium). Funding for the DPAC has been provided by national institutions, in particular the institutions participating in the *Gaia* Multilateral Agreement. This research made use of services provided by the Jean-Marie Mariotti Center (Aspro and SearchCal). The SIMBAD database, and NASA's Astrophysics Data System Bibliographic Services were used in the preparation of this paper. This work has made use of the High Contrast Data Centre, jointly operated by OSUG/IPAG (Grenoble), PYTHEAS/LAM/CeSAM (Marseille), OCA/Lagrange (Nice), Observatoire de Paris/LESIA (Paris), and Observatoire de Lyon/CRAL, and supported by a grant from Labex OSUG@2020 (Investissements d'avenir – ANR10 LABX56). This research has made use of the Spanish Virtual Observatory (https://svo.cab.inta-csic.es) project funded by MCIN/AEI/10.13039/501100011033/ through grant PID2020-112949GB-I00.

References

Amara, A., & Quanz, S. P. 2012, MNRAS, 427, 948
Anderson, R. I., Casertano, S., Riess, A. G., et al. 2016, ApJS, 226, 18
Babel, J., Burki, G., Mayor, M., Chmielewski, Y., & Waelkens, C. 1989, A&A, 216, 125
Balog, Z., & Vinko, J. 1995, Inf. Bull. Var. Stars, 4150, 1
Benedict, G. F., McArthur, B. E., Feast, M. W., et al. 2007, AJ, 133, 1810
Berdnikov, L. N. 2008, VizieR Online Data Catalog: II/285
Beuzit, J. L., Vigan, A., Mouillet, D., et al. 2019, A&A, 631, A155
Boccaletti, A., Chauvin, G., Mouillet, D., et al. 2020, ArXiv e-prints [arXiv:2003.05714]
Bohm-Vitense, E. 1985, ApJ, 296, 169
Böhm-Vitense, E., Remage Evans, N., Carpenter, K., Beck-Winchatz, B., & Robinson, R. 1997, ApJ, 477, 916
Chini, R., Hoffmeister, V. H., Nasseri, A., Stahl, O., & Zinnecker, H. 2012, MNRAS, 424, 1925
Csörnyei, G., Szabados, L., Molnár, L., et al. 2022, MNRAS, 511, 2125
Delorme, P., Meunier, N., & Albert, D. 2017, in SF2A-2017: Proceedings of the Annual meeting of the French Society of Astronomy and Astrophysics, eds. C. Reylé, P. Di Matteo, F. Herpin, et al., 347
Duchêne, G., & Kraus, A. 2013, ARA&A, 51, 269
Engler, N., Schmid, H. M., Quanz, S. P., Avenhaus, H., & Bazzon, A. 2018, A&A, 618, A151
Evans, N. R. 1988, ApJS, 66, 343
Evans, N. R. 1991, ApJ, 372, 597
Evans, N. R. 1992a, ApJ, 384, 220
Evans, N. R. 1992b, ApJ, 389, 657
Evans, N. R. 1994, ApJ, 436, 273
Evans, N. R. 1995, ApJ, 445, 393
Evans, N. R., Boehm-Vitense, E., Carpenter, K., Beck-Winchatz, B., & Robinson, R. 1998, ApJ, 494, 768
Evans, N. R., Carpenter, K. G., Robinson, R., Kienzle, F., & Dekas, A. E. 2005, AJ, 130, 789
Evans, N. R., Schaefer, G. H., Bond, H. E., et al. 2008, AJ, 136, 1137
Evans, N. R., Massa, D., & Proffitt, C. 2009, AJ, 137, 3700
Evans, N. R., Berdnikov, L., Gorynya, N., Rastorguev, A., & Eaton, J. 2011, AJ, 142, 87
Evans, N. R., Bond, H. E., Schaefer, G. H., et al. 2013, AJ, 146, 93
Evans, N. R., Berdnikov, L., Lauer, J., et al. 2015, AJ, 150, 13
Evans, N. R., Bond, H. E., Schaefer, G. H., et al. 2016, AJ, 151, 129
Evans, N. R., Karovska, M., Bond, H. E., et al. 2018a, ApJ, 863, 187
Evans, N. R., Proffitt, C., Carpenter, K. G., et al. 2018b, ApJ, 866, 30
Evans, N. R., Günther, H. M., Bond, H. E., et al. 2020, ApJ, 905, 81
Evans, N. R., Engle, S., Pillitteri, I., et al. 2022, ApJ, 938, 153
Evans, N. R., Proffitt, C., Kervella, P., et al. 2025, AJ, 170, 242
Fernie, J. D., Evans, N. R., Beattie, B., & Seager, S. 1995, Inf. Bull. Var. Stars, 4148, 1
Foreman-Mackey, D., Hogg, D. W., Lang, D., & Goodman, J. 2013, PASP, 125, 306
Fouqué, P., Arriagada, P., Storm, J., et al. 2007, A&A, 476, 73
Gaia Collaboration (Brown, A. G. A., et al.) 2018, A&A, 616, A1
Gallenne, A., Kervella, P., Mérand, A., et al. 2013, EAS Publ. Ser., 64, 197
Gallenne, A., Kervella, P., Mérand, A., et al. 2014a, A&A, 567, A60
Gallenne, A., Mérand, A., Kervella, P., et al. 2014b, A&A, 561, L3
Gallenne, A., Mérand, A., Kervella, P., et al. 2015, A&A, 579, A68
Gallenne, A., Kervella, P., Evans, N. R., et al. 2018, ApJ, 867, 121
Gallenne, A., Kervella, P., Borgniet, S., et al. 2019, A&A, 622, A164
Gerard, B. L., & Marois, C. 2016, SPIE Conf. Ser., 9909, 990958
Gieren, W. P. 1985, ApJ, 295, 507
Gieren, W., Storm, J., Konorski, P., et al. 2018, A&A, 620, A99
Gomez Gonzalez, C. A., Absil, O., Absil, P. A., et al. 2016, A&A, 589, A54
Gomez Gonzalez, C. A., Wertz, O., Absil, O., et al. 2017, AJ, 154, 7
Gorynya, N. A., Rastorguev, A. S., & Samus, N. N. 1996, Astron. Lett., 22, 33
Groenewegen, M. A. T. 2020, A&A, 635, A33
Harris, H. C. 1981, AJ, 86, 719
Harris, H. C., & Welch, D. L. 1989, AJ, 98, 981
Hocdé, V., Moskalik, P., Gorynya, N. A., et al. 2024, A&A, 689, A224
Jacobsen, T. S. 1974, ApJ, 191, 691
Keller, S. C. 2008, ApJ, 677, 483
Kervella, P., Nardetto, N., Bersier, D., Mourard, D., & Coudé du Foresto, V. 2004, A&A, 416, 941
Kervella, P., Arenou, F., Mignard, F., & Thévenin, F. 2019a, A&A, 623, A72
Kervella, P., Gallenne, A., Evans, N. R., et al. 2019b, A&A, 623, A117
Kervella, P., Gallenne, A., Remage Evans, N., et al. 2019c, A&A, 623, A116
Kervella, P., Arenou, F., & Thévenin, F. 2022, A&A, 657, A7
Kouwenhoven, M. B. N., Brown, A. G. A., Zinnecker, H., Kaper, L., & Portegies Zwart, S. F. 2005, A&A, 430, 137
Lafrenière, D., Marois, C., Doyon, R., Nadeau, D., & Artigau, É. 2007, ApJ, 660, 770
Lafrenière, D., Marois, C., Doyon, R., & Barman, T. 2009, ApJ, 694, L148
Lagrange, A. M., Bonnefoy, M., Chauvin, G., et al. 2010, Science, 329, 57
Lallement, R., Capitanio, L., Ruiz-Dern, L., et al. 2018, A&A, 616, A132
Laney, C. D. 1995, ASP Conf. Ser., 83, 367
Lee, D. D., & Seung, H. S. 1999, Nature, 401, 788
Lindegren, L., Bastian, U., Biermann, M., et al. 2021, A&A, 649, A4
Lloyd Evans, T. 1982, MNRAS, 199, 925
Marois, C., Lafrenière, D., Doyon, R., Macintosh, B., & Nadeau, D. 2006, ApJ, 641, 556
Marois, C., Macintosh, B., & Véran, J.-P. 2010, SPIE Conf. Ser., 7736, 77361J
Massa, D., & Evans, N. R. 2008, MNRAS, 383, 139
Mawet, D., Milli, J., Wahhaj, Z., et al. 2014, ApJ, 792, 97
Morgan, B. L., Beddoes, D. R., Scaddan, R. J., & Dainty, J. C. 1978, MNRAS, 183, 701
Neilson, H. R., & Lester, J. B. 2008, ApJ, 684, 569
Neilson, H. R., Cantiello, M., & Langer, N. 2011, A&A, 529, L9
Neilson, H. R., Schneider, F. R. N., Izzard, R. G., Evans, N. R., & Langer, N. 2015, A&A, 574, A2
Neilson, H. R., Engle, S. G., Guinan, E. F., Bisol, A. C., & Butterworth, N. 2016, ApJ, 824, 1
Pecaut, M. J., & Mamajek, E. E. 2013, ApJS, 208, 9
Percy, J. R., & Hoss, J. X. 2000, JAAVSO, 29, 14
Petterson, O. K. L., Cottrell, P. L., & Albrow, M. D. 2004, MNRAS, 350, 95
Pilecki, B., Graczyk, D., Gieren, W., et al. 2015, ApJ, 806, 29
Pilecki, B., Gieren, W., Pietrzyński, G., et al. 2018, ApJ, 862, 43
Schmid, H. M., Bazzon, A., Milli, J., et al. 2017, A&A, 602, A53
Schmid, H. M., Bazzon, A., Roelfsema, R., et al. 2018, A&A, 619, A9
Shetye, S. S., Viviani, G., Anderson, R. I., et al. 2024, A&A, 690, A284
Soummer, R., Hagan, J. B., Pueyo, L., et al. 2011, ApJ, 741, 55
Szabados, L. 1989, Commun. Konkoly Obs. Hungary, 94, 1
Szabados, L. 1991, Commun. Konkoly Obs. Hungary, 96, 123
Szabados, L. 2003, Inf. Bull. Var. Stars, 5394, 1
Szabados, L., & Nehéz, D. 2012, MNRAS, 426, 3148
Szabados, L., Anderson, R. I., Derekas, A., et al. 2013, MNRAS, 434, 870
Tokovinin, A., Mason, B. D., Mendez, R. A., Horch, E. P., & Briceño, C. 2019, AJ, 158, 48
Tokovinin, A., Mason, B. D., Mendez, R. A., Costa, E., & Horch, E. P. 2020, AJ, 160, 7
Trahin, B. 2019, Ph.D. Thesis, Université PSL
Trahin, B., Breuval, L., Kervella, P., et al. 2021, A&A, 656, A102
Turner, D. G. 2016, Rev. Mexicana Astron. Astrofis., 52, 223
Welch, D. L., Evans, N. R., Lyons, R. W., et al. 1987, PASP, 99, 610

Appendix A: Log of our SPHERE observations

Table A.1. Log of the SPHERE/ZIMPOL observations.

Star	UT	MJD (day)	Filter	NDF	DIT (s)	N_{DIT}	N_{exp}	Seeing (″)
η Aql	2018-05-25	58263.392	V/I'	ND2	1	20	6	0.61
η Aql	2018-05-25	58263.390	V/R'	ND2	1	20	6	0.65
FF Aql	2018-04-20	58228.394	V/I'	ND2	5	20	3	0.55
FF Aql	2018-04-20	58228.385	V/R'	ND2	5	20	6	0.65
FN Aql	2018-08-11	58341.224	V/I'	ND1	5	20	6	0.67
FN Aql	2018-08-11	58341.217	V/R'	ND1	5	20	6	0.53
KL Aql	2018-08-09	58339.250	V/I'	–	30	10	3	0.71
KL Aql	2018-08-09	58339.224	V/R'	–	30	10	6	0.99
V496 Aql	2018-08-10	58340.257	V/I'	ND1	4	20	6	0.51
V496 Aql	2018-08-10	58340.251	V/R'	ND1	4	20	6	0.75
V916 Aql	2018-07-11	58310.149	V/I'	ND1	60	8	3	0.48
V916 Aql	2018-07-11	58310.132	V/R'	ND1	60	8	3	0.61
V1344 Aql	2018-08-07	58337.237	V/I'	ND1	4	20	6	0.51
V1344 Aql	2018-08-07	58337.23	V/R'	ND1	4	20	6	0.50
V340 Ara	2018-08-17	58347.168	V/I'	ND1	40	8	3	0.58
V340 Ara	2018-08-17	58347.142	V/R'	ND1	40	9	6	0.61
GX Car	2020-01-28	58876.302	V/I'	–	5	20	9	0.95
GX Car	2020-01-28	58876.308	V/R'	–	5	20	9	0.84
U Car	2018-05-20	58258.147	V/I'	ND2	9	20	6	0.52
U Car	2018-05-20	58258.134	V/R'	ND2	9	20	6	0.68
UW Car	2020-01-28	58876.29	V/I'	–	5	20	9	0.77
UW Car	2020-01-28	58876.278	V/R'	–	5	20	9	0.95
V339 Cen	2018-07-11	58310.118	V/I'	ND1	8	20	3	0.47
V339 Cen	2018-07-11	58310.106	V/R'	ND1	8	20	6	0.38
V659 Cen	2018-07-03	58302.094	V/I'	ND1	2.5	20	3	1.49
V659 Cen	2018-07-03	58302.090	V/R'	ND1	2.5	20	6	1.56
AX Cir	2018-08-17	58347.049	V/I'	ND2	8.7	20	3	0.51
AX Cir	2018-08-17	58347.036	V/R'	ND2	8.7	20	6	0.61
RZ CMa	2020-02-23	58902.144	V/I'	–	3	20	12	0.61
RZ CMa	2020-02-23	58902.132	V/R'	–	8	10	12	1.16
TX Del	2018-07-14	58313.283	V/I'	–	3	100	3	0.49
TX Del	2018-07-14	58313.261	V/R'	–	3	100	6	0.57
β Dor	2020-01-17	58865.149	V/I'	ND2	3	20	9	0.57
β Dor	2020-01-17	58865.141	V/R'	ND2	3	20	9	0.78
T Mon	2020-02-15	58894.071	V/I'	ND1	2	20	15	0.46
T Mon	2020-02-15	58894.062	V/R'	ND1	1	40	15	0.53
TX Mon	2020-02-24	58903.144	V/I'	–	12	20	6	0.53
TX Mon	2020-02-24	58903.124	V/R'	–	12	20	6	0.68
V465 Mon	2020-03-23	58931.084	V/I'	–	12	20	6	0.65
V465 Mon	2020-03-23	58931.066	V/R'	–	12	20	6	0.65
S Nor	2018-08-17	58347.119	V/I'	ND1	1.2	20	3	0.54
S Nor	2018-08-17	58347.116	V/R'	ND1	1.2	20	6	0.53
BF Oph	2018-07-15	58314.231	V/I'	ND1	1.7	20	3	0.63
BF Oph	2018-07-15	58314.228	V/R'	ND1	1.7	20	6	0.55
Y Oph	2018-05-25	58263.376	V/I'	ND2	11	20	3	0.54
Y Oph	2018-05-25	58263.360	V/R'	ND2	11	20	6	0.76
AP Pup	2020-03-17	58925.114	V/I'	ND1	8	20	6	0.94
AP Pup	2020-03-17	58925.102	V/R'	ND1	8	20	6	1.0
X Pup	2020-03-17	58925.082	V/I'	–	2	60	9	1.28
X Pup	2020-03-17	58925.064	V/R'	–	2	60	9	1.11
RY Sco	2018-06-12	58281.274	V/I'	ND1	3	20	3	0.77
RY Sco	2018-06-12	58281.269	V/R'	ND1	3	20	6	0.86
RV Sco	2018-08-14	58344.097	V/I'	ND1	1.3	20	3	1.06
RV Sco	2018-08-14	58344.094	V/R'	ND1	1.3	20	6	1.15
V482 Sco	2018-08-14	58344.152	V/I'	ND1	4.3	20	3	0.65
V482 Sco	2018-08-14	58344.145	V/R'	ND1	4.3	20	6	0.69

Table A.1. continued.

V636 Sco	2018-08-07	58337.223	V/I'	ND1	3	10	3	0.51
V636 Sco	2018-08-07	58337.218	V/R'	ND1	1.5	20	6	0.51
RU Sct	2018-08-06	58336.251	V/I'	–	1	20	3	0.92
RU Sct	2018-08-06	58336.234	V/R'	–	5	40	6	1.02
Y Sct	2018-08-14	58344.194	V/I'	ND1	34	10	3	0.56
Y Sct	2018-08-14	58344.169	V/R'	ND1	34	10	6	0.58
BQ Ser	2018-08-14	58344.126	V/I'	ND1	30	10	3	0.73
BQ Ser	2018-08-14	58344.104	V/R'	ND1	30	10	6	0.93
S Sge	2018-05-25	58263.407	V/I'	ND2	5	20	3	0.73
S Sge	2018-05-25	58263.399	V/R'	ND2	5	20	6	0.54
AP Sgr	2018-06-14	58283.321	V/I'	–	1.3	20	3	0.36
AP Sgr	2018-06-14	58283.319	V/R'	–	1.3	20	6	0.46
BB Sgr	2018-06-14	58283.367	V/I'	ND1	1.5	20	3	0.74
BB Sgr	2018-06-14	58283.364	V/R'	ND1	1.5	20	6	0.77
U Sgr	2018-06-14	58283.332	V/I'	ND1	1.4	20	3	0.38
U Sgr	2018-06-14	58283.33	V/R'	ND1	1.4	20	6	0.40
V350 Sgr	2018-08-10	58340.241	V/I'	ND1	3	20	3	0.54
V350 Sgr	2-19-08-10	58340.234	V/R'	ND1	3	20	6	0.54
W Sgr	2018-06-12	58281.288	V/I'	ND2	2.6	20	3	0.78
W Sgr	2-18-06-12	58281.284	V/R'	ND2	2.6	20	6	0.69
WZ Sgr	2018-08-11	58341.207	V/I'	ND1	3	20	3	0.75
WZ Sgr	2018-08-11	58341.202	V/R'	ND1	3	20	6	0.88
X Sgr	2018-07-17	58316.256	V/I'	ND2	2.2	20	3	0.90
X Sgr	2018-07-17	58316.252	V/R'	ND2	2.2	20	6	1.29
Y Sgr	2018-06-14	58283.352	V/I'	ND2	7.3	20	3	0.48
Y Sgr	2018-06-14	58283.341	V/R'	ND2	7.3	20	6	0.37
YZ Sgr	2018-08-07	58337.254	V/I'	ND2	4	10	3	0.45
YZ Sgr	2018-08-07	58337.25	V/R'	ND2	4	10	6	0.45
LR Tra	2018-06-11	58280.155	V/I'	ND1	4	20	3	0.74
LR Tra	2018-06-11	58280.148	V/R'	ND1	4	20	6	0.79
R Tra	2018-07-11	58310.097	V/I'	ND1	1.1	20	3	0.37
R Tra	2018-07-11	58310.094	V/R'	ND1	1.1	20	6	0.41
RZ Vel	2020-01-18	58866.195	V/I'	ND1	4	30	9	0.30
RZ Vel	2020-01-18	58866.179	V/R'	ND1	6	20	9	0.40
V Vel	2020-01-19	58867.154	V/I'	ND1	8	30	6	0.44
V Vel	2020-01-19	58867.146	V/R'	ND1	10	6	6	0.47
T Vel	2020-01-18	58866.156	V/I'	ND1	12	20	6	0.46
T Vel	2020-01-18	58866.138	V/R'	ND1	12	20	6	0.88

Notes. NDF: neutral density filter (attenuation factor of $\sim$ 12 and $\sim$ 120, respectively for ND1 and ND2). DIT: detector integration time. N_{exp}: number of exposure.